Received: 12 January 2024 | Revised: 20 February 2024 | Accepted: 21 February 2024

DOI: 10.1002/pol.20240030

RESEARCH ARTICLE

JOURNAL OF POLYMER SCIENCE WILEY

Self-assembly of supramolecular monomers into 2D twinned crystals on mica surface

Elisabeth Weyandt[1] | **Francesco Simone Ruggeri**[2,3] | **E. W. Meijer**[1] | **Ghislaine Vantomme**[1]

[1]Institute for Complex Molecular Systems (ICMS) and Laboratory of Macromolecular and Organic Chemistry, Eindhoven University of Technology, Eindhoven, The Netherlands

[2]Laboratory of Organic Chemistry, Wageningen University, Wageningen, The Netherlands

[3]Physical Chemistry and Soft Matter, Wageningen University, Wageningen, The Netherlands

Correspondence
Ghislaine Vantomme, Institute for Complex Molecular Systems (ICMS) and Laboratory of Macromolecular and Organic Chemistry, Eindhoven University of Technology, P.O. Box 513, 5600 MB Eindhoven, The Netherlands.
Email: g.vantomme@tue.nl

Funding information
HORIZON EUROPE European Research Council, Grant/Award Number: 788618; Ministerie van Onderwijs, Cultuur en Wetenschap, Grant/Award Numbers: IPM 024.005.020, OCENW.M20.256

Abstract

Despite the widespread use of microscopy techniques to characterize supramolecular polymers, the role of surfaces in the formation of these structures is unclear. Here we describe the epitaxial growth of intriguing 2D crystals of alkyl benzene-1,3,5-triscarboxamides formed by competitive attractive interactions with the mica surface. In contrast to the fibrous structure observed in apolar diluted solution, five-fold twinned crystals or ribbon-like structures are obtained on the mica surface. Moreover, these structures are still dynamic on the surface, being able to reorganize during the atomic force microscopy measurements. This work demonstrates that surface-monomer interactions can be exploited to modulate the structure of 1D supramolecular polymers into 2D crystals.

KEYWORDS

epitaxy, pathway complexity, polymorphism, supramolecular polymers

1 | INTRODUCTION

The assembly of supramolecular polymers in solution has been well explored in recent years, showing how molecular design and sample preparation can influence pathway complexity in these systems.[1] In solution, the morphology of supramolecular polymers is governed by the interplay of non-covalent monomer–monomer interactions in combination with the solvation of the aggregates in the solvent.[2–5] For example, benzene-1,3,5-triscarboxamides (BTAs) polymerize into helical 1D supramolecular fibers stabilized by trifold hydrogen bonding, π-stacking and solvent interactions (Figure 1A,B).[6] In fact, the solvation of these amphiphilic building blocks results from a subtle balance of solvophobic interactions of the core and solvophilic interactions of the periphery, and contributes to their dynamic properties and ability to form ordered helical structures in solution. Numerous studies have reported on the influence of this subtle balance on the assembly mechanism and aggregate morphology by iterative variations in BTAs structure,[3,7,8] assembly in different solvents[4,9–11] and, more recently, copolymerizations.[12,13] By the correct selection of surfaces many of these supramolecular polymers, first made in solution, can be visualized by

surface techniques like atomic force microscopy (AFM) either as individual polymer chains or as bundles of these polymers.[14]

However, the self-assembly of these monomers on surfaces remains puzzling and unpredictable. When bringing supramolecular systems from a solution to a surface, not only monomer-monomer interactions have to be considered, but also monomer-surface interactions, solvent interactions, and solvent evaporation kinetics. Therefore, achieving long range macroscopic order through self-assembly on a surface remains a challenge, as structure formation is governed by the competition of interactions, surface-induced conformational changes, and molecular packing.[15] Nevertheless, long-range ordered self-assembled monolayers[16,17] are a topic of major interest for applications in biomedicine, nanoelectronics, and photovoltaic devices.

Recently, significant progress has been made in understanding surface effects on the formation of supramolecular structures.[18,19] Many previously unknown crystal polymorphs are discovered when the crystallization process occurs on a surface rather than through a nucleation process in solution.[20–22] Epitaxy is defined as the growth of a crystalline material on another crystal and where the epitaxial layer is in registry with the substrate. The crystallinity of the substrate material can thus be used to dictate the order of a deposited layer. For conjugated organic molecules, solution-phase deposition is the most commonly used method to generate ordered films for semiconductors.[23] For example, the π-conjugated cores of small molecules adsorb strongly onto HOPG surfaces and alkyl chains form large ordered domains around the cores.[15,24,25] However, only a few examples exist of small organic molecules with long flexible side chains or linkers, often used in supramolecular polymerizations.[26]

Here we report the formation of intriguing 2D polygon-shaped crystals of achiral, alkyl BTAs **C_6-BTA, C_8-BTA,** and **C_{10}-BTA** on crystalline, atomically flat mica surfaces (Figure 1). Instead of the 1D supramolecular fibers characterized in solution by static light scattering,[27,28] flat pentagons structures with a highly geometric appearance or ribbon-like structures are observed on a mica substrate by atomic force microscopy (AFM) (Figure 1C, Figures S1–S3). The monomer-surface interactions overrule the monomer-monomer interactions, leading to the epitaxial growth of ordered 2D crystals. We study the influence of the side chain length of the monomers and the nature of the surface on the morphology of structures deposited on the surface by AFM.

2 | RESULTS AND DISCUSSION

2.1 | 2D crystal formation observed for C_6-BTA, C_8-BTA, and C_{10}-BTA

To our surprise, we found that achiral alkyl BTAs drop-casted on mica do not exhibit a fibrous morphology as seen from previous studies,[27–29] but form highly geometric 2D crystals (Figure 2, details on sample preparation in SI). One of these polygons is shown in Figure 1C, and features five triangular crystal planes with a uniform height of about 1.5 nm and the tip reaches up to 5 nm. The width of these polygon-shaped crystals varies from several hundred nanometers to a few micrometers. In the middle of the polygon there is often a hole or a "spike"-like structure of varying height (Figure 2 and Figure S1). Moreover, these structures seem to orient following the triangular symmetry of the mica substrate, suggesting epitaxial growth. This intriguing assembly occurs for BTAs with six up to 10 carbon atoms in the side chain (Figure 2A–C). For longer alkyl chains of 12 carbons, we observed the formation of needle-like 3D crystals (Figure 2D).

The most common shape of the 2D crystals is a pentagon, although higher-order symmetries are also

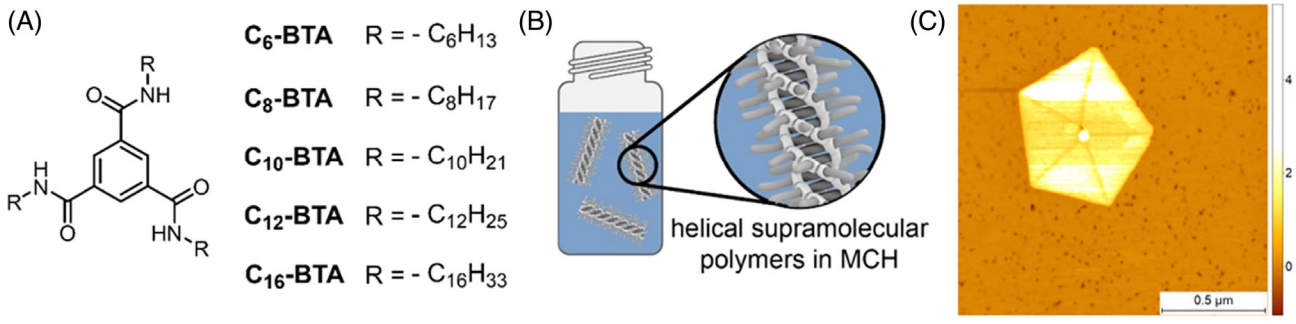

FIGURE 1 (A) Structure of alkyl benzene-1,3,5-triscarboxamides (BTAs) **C_n-BTA** with chain lengths of 6 to 16 carbon atoms. (B) Alkyl BTAs assemble into 1D helical supramolecular fibers in a dilute apolar solution of methylcyclohexane (MCH). (C) 2D crystal polygons of **C_8-BTA** on a flat crystalline mica surface observed by atomic force microscopy (AFM), with height analysis showing a uniform height of around 1.5 nm and a spike reaching up to 5 nm.

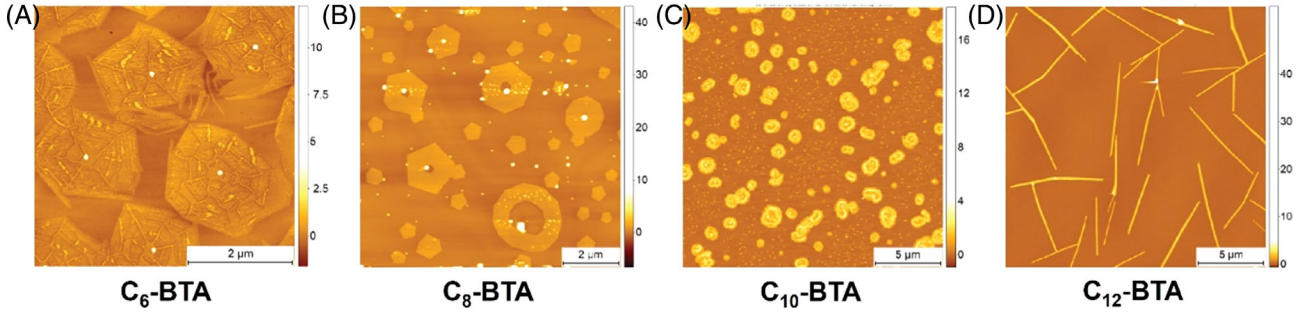

FIGURE 2 The structures formed on mica with **C_6-BTA** (A), **C_8-BTA** (B), **C_{10}-BTA** (C), and **C_{12}-BTA** (D). All samples were dropcasted from 20 µM solutions in MCH.

observed (Figure S2). The rotational symmetry of a crystal is usually limited to 2-fold, 3-fold, 4-fold, or 6-fold, while 5-fold symmetry has so far only been observed for quasicrystals.[30,31] Here, the overall 5-fold symmetry of the pentagon-shaped structures originates from a 5-fold twinning of the crystal phases, meaning the 2D crystals consist of five triangular crystal planes of the same crystal lattice, but with different orientation in the 2D plane. Very few examples of 5-fold twinning exist for the growth of inorganic metal nanorods,[32,33] and to our knowledge, only one example has been reported for an organic nanostructure.[34] The crystalline morphology found on the surface is often polygon-shaped, but ribbon-like structures can also be observed (Figure S3). These ribbon structures also exhibit the spike and often follow a roughly triangular structure likely derived from the mica crystal lattice (Figure S3a). The structure that forms is most likely governed by a multitude of external factors such as humidity, temperature, solvent evaporation, and changes in local concentration on the surface. The experiments were repeated several times and surfaces dominated by polygonal structures and sometimes ribbon-shaped crystals were obtained with the same procedure of sample preparation, showing the delicate interplay of interactions to grow these structures. Figure S3b shows the transition from ribbon to polygonal structures.

To elucidate molecular packing in these thin 2D crystals, we performed high-resolution, phase-controlled AFM,[35,36] to obtain a quantitative height analysis of the crystals grown from **C_8-**, **C_{12}-**, and **C_{16}-BTA** (see details in SI, Figure 3). For **C_8-BTA** ribbons on mica, we found an average height of the smallest ribbons of 1.3 ± 0.1 nm and a width of around 150 nm (Figure 3A,B). To deduce the number of monomers forming a single ribbon, we measured the 3D shape and size of the **C_8-BTA** structures, which displayed a typical height of 0.6 ± 0.1 nm and a width of approximately 75 nm (Figure S4). Measurements of the monomer units suggest that the ribbons cross-section contains four monomers in a rectangular arrangement, i.e. two layers of two monomers, indicating a possible lateral packing of BTA monomers on the mica surface. For **C_{12}-BTA**, the ribbons exhibited an average height of 1.9 ± 0.1 nm and a typical larger width linked to the increase in the alkyl chain. Within these ribbons, highlands with another layer of monomers were sometimes observed, resulting in a final height of 2.4 ± 0.1 nm (Figure 3C,D and Figure S5). **C_{16}-BTA** crystals also showed a clear monodirectional nematic organization with periodicity of around 70 nm and height of 2.5 ± 0.4 nm (Figure S6). In addition, multiple layers were sometimes observed, producing much taller structures of up to 6.5–7 nm (Figure 3E,F and Figure S6).

BTA polymorphism can explain the differences observed between bulk and surface assemblies. Indeed, BTA monomers can form hydrogen bonds both laterally (thermodynamic polymorph) and columnarly (kinetic polymorph). In variable temperature IR experiments, this transition becomes visible as a shift of the NH-band from $\nu = 3307\ \mathrm{cm}^{-1}$ for the lateral hydrogen-bonded polymorph to $\nu = 3250\ \mathrm{cm}^{-1}$ for the columnar polymorph (Figure S7). The presence of two different crystal structures for these BTAs suggests some conformational flexibility in the molecular packing in bulk, which could explain the appearance of the 2D polygon crystals formed on mica. A chiral **C_8-BTA** nanosheet connected by lateral hydrogen bonds was reported by Chu et al. with a thickness of 1.8 nm in water.[37] The height of the 2D crystals we observed in air is about 0.5 nm lower than the one found for lateral packing by Chu et al. in water. The reduced height in air correlates with tighter packing of the side chains in air than in liquid, as well as with the influence of the Hamaker constant of the mica substrate during measurements in air, as observed for DNA measurements.[38] However, we could also not exclude the formation of another polymorph on mica.[33] Unfortunately, as the crystals were very thin and formed only on a crystalline surface, it was not possible to further characterize the molecular packing using high-resolution analytical

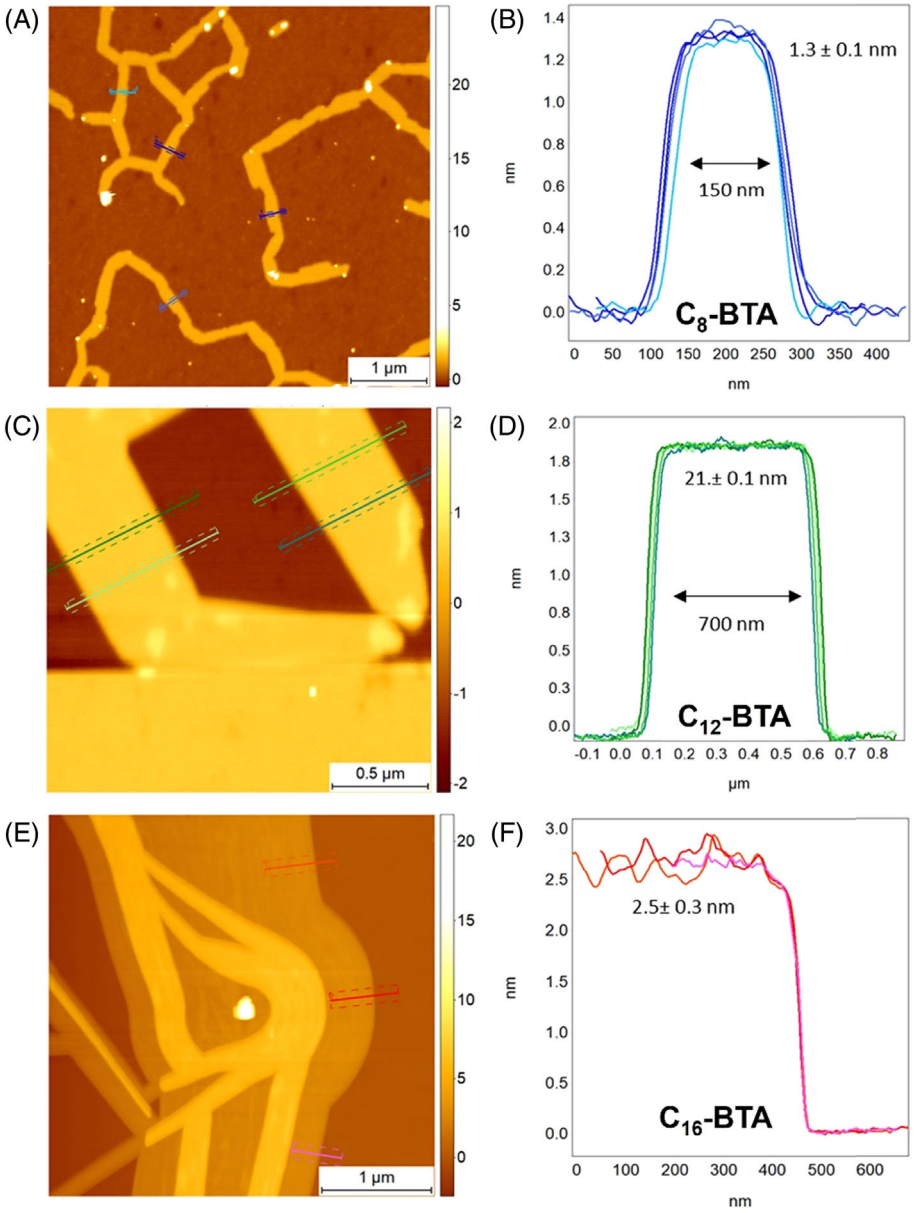

FIGURE 3 High-resolution and phase-controlled maps of ribbons and their cross-sectional dimensions on mica for (A and B) $\mathbf{C_8}$-, (C and D) $\mathbf{C_{12}}$-, and (E and F) $\mathbf{C_{16}}$-**BTA.**

techniques. Nevertheless, further characterization was carried out by studying the influence of surface and supramolecular motif on the structures obtained in the following paragraph.

2.2 | Structure formation strongly dependent on surface

The influence of the surface on the formation of these structures was then evaluated. Both HOPG and glass surfaces were tested, and the growth of highly geometric polygonal crystals was only observed for mica surfaces (Figure 4). Remarkably, on all surfaces tested, we did not observe fibrous structures for $\mathbf{C_8}$-**BTA**, indicating that this morphology is energetically unfavorable on surface, as was shown in the bulk phase.[39] When dropcasting $\mathbf{C_8}$-**BTA** on HOPG, we observed a fingerprint pattern in the background with 3D islands growing up to a height of 10 nm. HOPG is a strongly adsorptive surface for organic molecules due to its large π surface area. First, monolayers are formed from molecules adsorbed flat on HOPG, then 2D and 3D crystals grow on the initial monolayer.[40] The visible fingerprint on the surface is most likely a layer of BTA monomers adsorbed onto the graphite surface by π-stacking and van der Waals interactions. The structures observed after dropcasting $\mathbf{C_8}$-**BTA** on glass were mainly amorphous with no visible degree of order. The 2D crystals therefore formed only on mica surfaces, indicating an epitaxial growth mechanism with good surface registry. We speculate that BTA monomers align with the symmetry of the

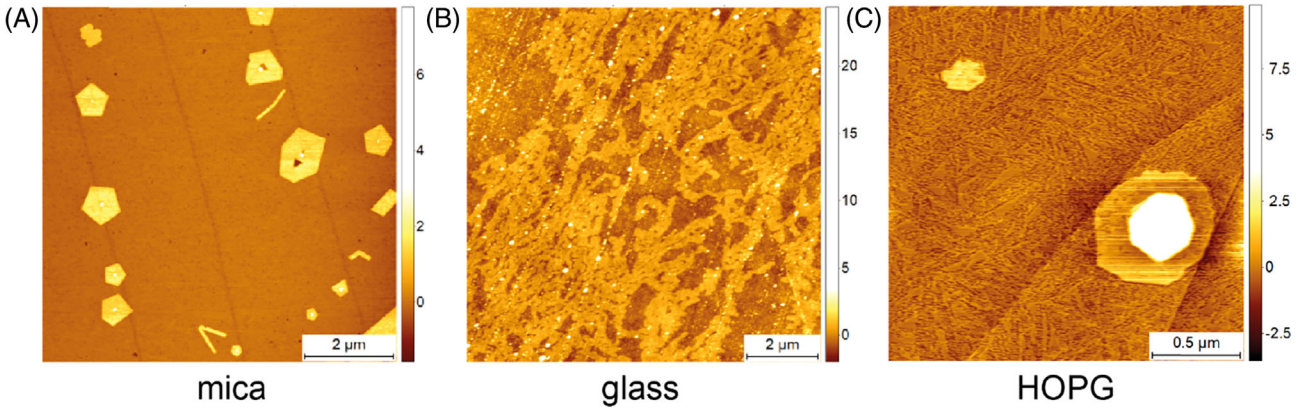

FIGURE 4 Crystal morphologies of **C_8-BTA** on mica (A), HOPG (B), and glass (C).

surface on which they crystallize and follow the three-fold symmetry of the substrate. Hence, the formation of these structures is specific to mica surfaces, and does not occur on other surface materials. This example demonstrates that the surface used in AFM experiments can have a major influence on the morphologies observed, even though it is generally considered to be innocent in the structure formation of supramolecular materials.

We then investigated the assembly of other well-described hydrogen-bonded supramolecular building blocks on the mica surface (Figure S8). Similarly, epitaxially grown crystals were observed for these three motifs on both mica and HOPG surfaces. For bis(hexylureido)toluene (**HUT**), the formation of triangular crystalline phases on HOPG after vapor annealing and reorganization on the surface has been reported.[15] On mica, **HUT** assembled into flat sheets, which aligned very loosely in lines parallel to the surface (Figure S8a). For ***S*-PyPyTA** on mica, both heart- or drop-shaped crystals were found, some bearing spikes in the middle of the crystal similar to the polygonal crystals of **C_8-BTA** on mica (Figure S8b). Unlike the later, ***S*-PyPyTA** crystals appeared to be composed of a single crystal plane rather than twinned crystal phases on mica. Due to the uniform flatness of the drop-shaped crystals, the molecular packing on the surface is probably similar to **C_8-BTA**, although the chiral side chains hinder the formation of 2D geometric crystals. Finally, for the perfluorinated BTA monomer **perfl-BTA** on HOPG, we found long ribbon-like crystals aligned in a triagonal way with the underlying HOPG surface (Figure S8c). Beneath the ribbons, another layer of molecules adsorbed to the surface is visible, as evidenced by the deeper holes visible on parts of the surface. Due to their dynamic nature, supramolecular monomers appear to interact strongly with hydrophilic or strongly adsorbing surfaces such as mica and HOPG, leading to the formation of intriguing 2D ordered crystals.

2.3 | Metastable 2D assembly

We have also investigated the stability of these structures over time during AFM measurements. Although crystalline dropcasted structures on the surface are usually considered static, we observe changes in the structures attributed to the dynamicity of non-covalent interactions. When continuously scanning a dry sample of **C_6-BTA** for 12 h, we found that the 2D flat crystal planes formed by **C_6-BTA** were slowly consumed and transformed into 3D needle-like crystals growing on the surface (Figure 5).

The sample shown in Figure 5 was recrystallized by adding a few drops of methylcyclohexane (MCH), then dried and imaged. On the first scan (0 h), flat 1.5 nm crystal planes were visible, the same height as the polygons. With continuous scanning, the needles began to grow and spread across the entire image surface. After 12 hours, all the 2D flat crystals were consumed and only the needles were visible on the surface. A scan of nearby areas showed mostly 2D crystals and only a few needles (data not shown). Thus the mobility of molecules on the surface in the absence of solvent, but in presence of the typical hydration layers on a surface in air environment, and the laser heat, appears to be much higher than expected and is significant enough for molecules to migrate on the mica surface. Mobility due to tip movement was excluded because the same area scanned in non-contact mode showed no reorganization during single/multiple map acquisition. **C_6-BTA** monomer also exhibited a liquid crystalline phase in the temperature range of 50–200°C, which could explain the mobility of molecules on the surface. We hypothesize that the 2D crystals may be a metastable

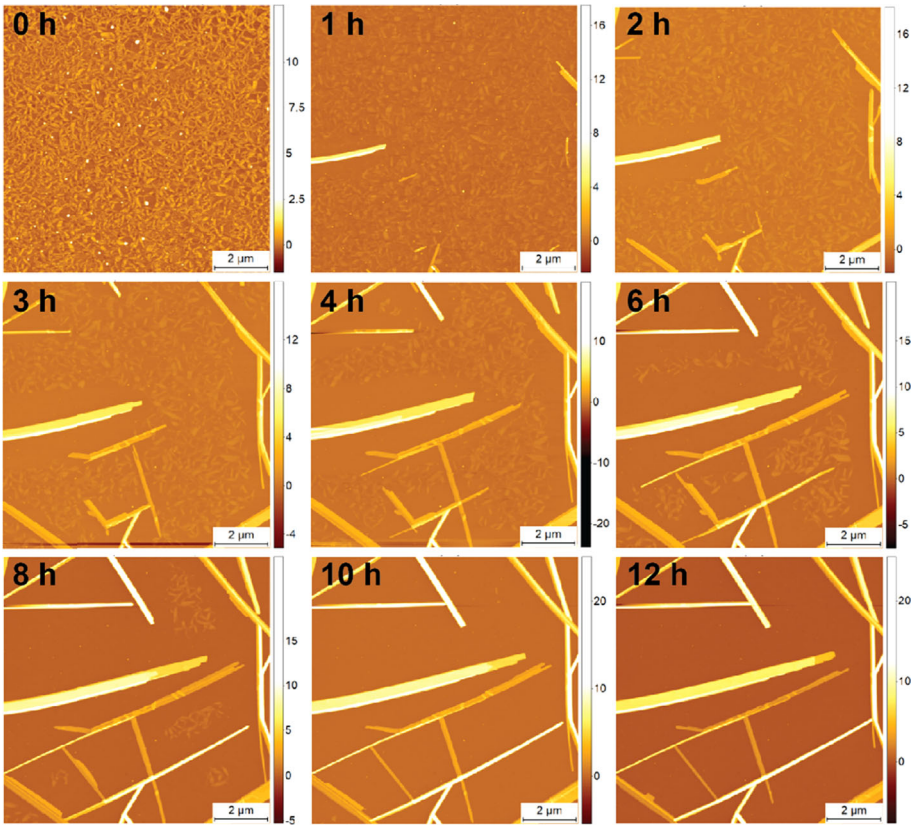

FIGURE 5 Time-resolved atomic force microscopy (AFM) images of **C6-BTA** on a mica surface over the course of 12 hours.

polymorph that transforms over time into a thermodynamically more stable polymorph.

The present work represents a step forward in the efforts to make ordered 2D materials, but it also highlights the challenges of characterizing supramolecular polymers by microscopy. The nature of surfaces influences supramolecular aggregation, while the noncovalent bonds holding the aggregates together are dynamic, by which pathway complexity can be observed with different morphologies as a result.

ACKNOWLEDGMENTS

The work received funding from the European Research Council (H2020-EU.1.1., SYNMAT project, ID 788618) and the Dutch Ministry of Education, Culture and Science (Gravitation Program IPM 024.005.020, OCENW.M20.256).

ORCID

Ghislaine Vantomme https://orcid.org/0000-0003-2036-8892

REFERENCES

[1] J. Matern, Y. Dorca, L. Sánchez, G. Fernández, *Angew. Chem., Int. Ed.* **2019**, *58*, 16730.
[2] M. F. J. Mabesoone, A. R. A. Palmans, E. W. Meijer, *J. Am. Chem. Soc.* **2020**, *142*, 19781.
[3] N. Veling, R. Van Hameren, A. M. Van Buul, A. E. Rowan, R. J. M. Nolte, J. A. A. W. Elemans, *Chem. Commun.* **2012**, *48*, 4371.
[4] J. S. Valera, R. Sánchez-Naya, F. J. Ramírez, J. L. Zafra, R. Gómez, J. Casado, L. Sánchez, *Chem. A Eur. J.* **2017**, *23*, 11141.
[5] T. Shimada, Y. Watanabe, T. Kajitani, M. Takeuchi, Y. Wakayama, K. Sugiyasu, *Chem. Sci.* **2023**, *14*, 822.
[6] S. Cantekin, T. F. A. De Greef, A. R. A. Palmans, *Chem. Soc. Rev.* **2012**, *41*, 6125.
[7] B. Narayan, C. Kulkarni, S. J. George, *J. Mater. Chem. C* **2013**, *1*, 626.
[8] L. López-Gandul, A. Morón-Blanco, F. García, L. L. Sánchez, *Angew. Chem. Int. Ed.* **2023**, *62*, e202308749.
[9] G. Ghosh, S. Ghosh, *Chem. Commun.* **2018**, *54*, 5720.
[10] K. Yano, T. Hanebuchi, X. J. Zhang, Y. Itoh, Y. Uchida, T. Sato, K. Matsuura, F. Kagawa, F. Araoka, T. Aida, *J. Am. Chem. Soc.* **2019**, *141*, 10033.
[11] N. Bäumer, K. K. Kartha, J. P. Palakkal, G. Fernández, *Soft Matter* **2020**, *16*, 6834.
[12] A. R. A. Palmans, E. W. Meijer, *Angew. Chem. Int. Ed.* **2007**, *46*, 8948.
[13] Y. Li, A. Hammoud, L. Bouteiller, M. Raynal, *J. Am. Chem. Soc.* **2020**, *142*, 5676.
[14] Y. Liu, Z. Wang, X. Zhang, *Chem. Soc. Rev.* **2012**, *41*, 5922.
[15] R. Shokri, F. Vonau, M. Cranney, D. Aubel, A. Narladkar, B. Isare, L. Bouteiller, L. Simon, G. Reiter, *J. Phys. Chem. C* **2012**, *116*, 21594.
[16] S. Casalini, C. A. Bortolotti, F. Leonardi, F. Biscarini, *Chem. Soc. Rev.* **2017**, *46*, 40.

[17] A. M. Travaille, L. Kaptijn, P. Verwer, B. Hulsken, J. A. A. W. Elemans, R. J. M. Nolte, H. Van Kempen, *J. Am. Chem. Soc.* **2003**, *125*, 11571.
[18] K. S. Mali, N. Pearce, S. De Feyter, N. R. Champness, *Chem. Soc. Rev.* **2017**, *46*, 2520.
[19] J. Labella, G. Lavarda, L. Hernández-López, F. Aguilar-Galindo, S. Díaz-Tendero, J. Lobo-Checa, T. Torres, *J. Am. Chem. Soc.* **2022**, *144*, 16579.
[20] H. Moshe, G. Levi, Y. Mastai, *CrystEngComm* **2013**, *15*, 9203.
[21] H. M. A. Ehmann, O. Werzer, *Cryst. Growth des.* **2014**, *14*, 3680.
[22] C. Yao, S. Zhang, L. Wang, X. Tao, *Cryst. Growth Des.* **2023**, *23*, 637.
[23] P. G. Evans, J. W. Spalenka, *Handbook of Crystal Growth: Thin Films and Epitaxy*, 2nd ed., Vol. 3, Elsevier Inc., Amsterdam **2015**, p. 509.
[24] S. Varghese, S. Fredrich, G. Vantomme, S. R. Prabhu, J. Teyssandier, S. De Feyter, J. Severn, C. W. M. Bastiaansen, A. P. H. J. Schenning, *J. Mater. Chem. C* **2020**, *8*, 694.
[25] D. Bléger, A. Bocheux, D. Kreher, F. Mathevet, A. J. Attias, G. Metgé, L. Douillard, C. Fiorini-Debuisschert, F. Charra, *Nanoscale* **2013**, *5*, 1452.
[26] Y. Zhu, W. Chen, T. Wang, H. Wang, Y. Wang, D. Yan, *J. Phys. Chem. B* **2016**, *120*, 4310.
[27] G. Vantomme, G. M. ter Huurne, C. Kulkarni, H. M. M. ten Eikelder, A. J. Markvoort, A. R. A. Palmans, E. W. Meijer, *J. Am. Chem. Soc.* **2019**, *141*, 18278.
[28] G. M. ter Huurne, P. Chidchob, A. Long, A. Martinez, A. R. A. Palmans, G. Vantomme, *Chem. A Eur. J.* **2020**, *26*, 9964.
[29] D. Kluge, J. C. Singer, J. W. Neubauer, F. Abraham, H. W. Schmidt, A. Fery, *Small* **2012**, *8*, 2563.
[30] D. L. D. Caspar, E. Fontano, *Proc. Natl. Acad. Sci.* **1996**, *93*, 14271.
[31] M. Křížek, J. Šolc, A. Šolcova, *Am. Math. Soc.* **2012**, *59*, 22.
[32] J. Yoon, N. T. Khi, H. Kim, B. Kim, H. Baik, S. Back, S. Lee, S. W. Lee, S. J. Kwon, K. Lee, *Chem. Commun.* **2013**, *49*, 573.
[33] H. Hofmeister, *Encycl. Nanosci. Nanotechnol.* **2003**, *3*, 431.
[34] L. Zheng, J. Liu, Y. Han, *Phys. Chem. Chem. Phys.* **2013**, *15*, 1208.
[35] F. S. Ruggeri, S. Vieweg, U. Cendrowska, G. Longo, A. Chiki, H. A. Lashuel, G. Dietler, *Sci. Reports* **2016**, *6*, 1.
[36] F. S. Ruggeri, T. Šneideris, M. Vendruscolo, T. P. J. Knowles, *Arch. Biochem. Biophys.* **2019**, *664*, 134.
[37] X. Hou, M. Schober, Q. Chu, *Cryst. Growth Des.* **2012**, *12*, 5159.
[38] F. S. Ruggeri, F. Benedetti, T. P. J. Knowles, H. A. Lashuel, S. Sekatskii, G. Dietler, *Proc. Natl. Acad. Sci. U. S. A.* **2018**, *115*, 7230.
[39] P. J. M. Stals, M. M. J. Smulders, R. Martín-Rapún, A. R. A. Palmans, E. W. Meijer, *Chem. A Eur. J.* **2009**, *15*, 2071.
[40] C. Fu, H. P. Lin, J. M. Macleod, A. Krayev, F. Rosei, D. F. Perepichka, *Chem. Mater.* **2016**, *28*, 951.

SUPPORTING INFORMATION

Additional supporting information can be found online in the Supporting Information section at the end of this article.

How to cite this article: E. Weyandt, F. S. Ruggeri, E. W. Meijer, G. Vantomme, *J. Polym. Sci.* **2024**, 1. https://doi.org/10.1002/pol.20240030